

UKAEA-CCFE-PR(25)339

I. Voitsekhovitch, M. Poradzinski, D. Taylor, A.  
Chomiczewska, H. Dudding, I. Ivanova-Stanik, D.  
King, M. Maslov, C. Roach

# **Particle and thermal transport in JET Helium and Hydrogen-Helium H- mode plasmas**

Enquiries about copyright and reproduction should in the first instance be addressed to the UKAEA Publications Officer, Culham Science Centre, Building K1/O/83 Abingdon, Oxfordshire, OX14 3DB, UK. The United Kingdom Atomic Energy Authority is the copyright holder.

The contents of this document and all other UKAEA Preprints, Reports and Conference Papers are available to view online free at [scientific-publications.ukaea.uk/](https://scientific-publications.ukaea.uk/)

# **Particle and thermal transport in JET Helium and Hydrogen-Helium H-mode plasmas**

I. Voitsekhovitch, M. Poradzinski, D. Taylor, A. Chomiczewska, H. Dudding, I. Ivanova-Stanik, D. King, M. Maslov, C. Roach



# Particle and thermal transport in JET Helium and Hydrogen-Helium H-mode plasmas

I. Voitsekhovitch<sup>1</sup>, M. Poradzinski<sup>2</sup>, D. Taylor<sup>1</sup>, A. Chomiczewska<sup>2</sup>, H. Dudding<sup>1</sup>, I. Ivanova-Stanik<sup>2</sup>, D. King<sup>1</sup>, M. Maslov<sup>1</sup>, C. Roach<sup>1</sup>, JET contributors\* and the EUROfusion Tokamak Exploitation Team\*\*

EUROfusion Consortium, JET, Culham Science Centre, Abingdon, OX14 3DB, UK

<sup>1</sup>UKAEA (United Kingdom Atomic Energy Authority), Culham Campus, Abingdon, Oxfordshire, OX14 3DB, UK

<sup>2</sup>Institute of Plasma Physics and Laser Microfusion, Hery Str. 23, 01-497, Warsaw, Poland

\*See the author list of J. Mailloux et al. 2022 Nucl. Fusion <https://doi.org/10.1088/1741-4326/ac47b4>

\*\*See the author list of E. Joffrin et al 2024 Nucl. Fusion **64** 112019  
<https://doi.org/10.1088/1741-4326/ad2be4>

## Abstract

Fusion performance in a tokamak-reactor strongly depends on the confinement of thermalised  $\alpha$ -particles (Helium (He) ash) in the core plasma region. Consequently, the development of He particle transport models and their validation in present experiments is an important step towards a more accurate prediction of fusion power production in future devices. In the absence of a computationally fast well-validated theory-based transport models for He, the empirical Bohm-gyroBohm (BgB) model is tested here for the first time to our knowledge in the predictive self-consistent temperature and density simulations of JET H-mode He and Hydrogen (H) - He discharges. The thermal confinement in JET He plasmas is found to be well below the Deuterium (D) BgB model reference – this result is qualitatively consistent with the observation of reduced global thermal confinement in He discharges observed on ASDEX

Upgrade, Cmod, DIII-D and EAST tokamaks compared to the confinement of D plasmas. The “Helium” version of the BgB model including the re-calibrated BgB thermal diffusivity and the He particle diffusion coefficient defined as a fixed fraction of the thermal electron diffusivity is proposed here. This model is validated in the JET discharges performed at different toroidal magnetic fields, plasma densities, wall materials (Carbon and ITER-like wall) and main ion compositions. Strong reduction of He particle transport with the increase of magnetic field has been found in JET discharges. However, the simulations of the He ash accumulation in the future high-field tokamak-reactor ARC with the model validated in JET predict a tolerable amount of He content in the burn phase in the broad parameter space, with a weak impact on the fusion power production. Similar conclusion has been drawn for the H-mode EU-DEMO scenario by extrapolating the JET He particle transport model to this device.

## I. Introduction

Experimental studies of Helium (He) plasmas performed on various tokamaks [1-10] have been motivated by their potential application in the non-nuclear commissioning phase of tokamak-reactors. The energy confinement in these plasmas has been extensively studied in a number of experiments using different heating schemes and He plasma purity [1-9]. The applied heating techniques vary from the He [1, 2, 6-8] and Hydrogen (H) [3] Neutral Beam Injection (NBI) into He plasmas, combined H beams and Electron Cyclotron Resonance Heating (ECRH) [3, 9] and pure radio frequency heating including ECRH [3], Ion Cyclotron Resonance Heating (ICRH) of H minority [4] and combined Lower Hybrid Current Drive (LHCD) and ECRH [5]. The He plasma purity was not the same in these experiments as the plasma dilution by Hydrogen is unavoidable when using the H beams [3] and H minority heating [4]. In spite of the variety of experimental conditions the conclusion on the global energy confinement in He plasmas was qualitatively the same in these experiments: the He energy confinement time ( $\tau_E$ ) is below the Deuterium (D) confinement time by up to 30% in the H-mode regime. It was found that Hydrogen also contributes to the confinement deterioration. Still few exceptions from this behaviour have been found: e.g. the experiments performed on AUG [9] show that the confinement of He plasmas increases with increasing fraction of electron heating, reaching the values comparable to those of the D plasmas.

The analysis of He experiments described above has been focused on the global energy confinement, while another important issue – a local He particle transport in the plasma core – was not addressed. An extensive study of the core He particle transport in D plasma where Helium constitutes a part of intrinsic impurity (He concentration was below 1.5%) coming from the wall, pre-coated by Helium during boronisation, has been performed on ASDEX-Upgrade [10]. Broad engineering and physics parameters space has been explored in this work showing that the He density profile shape follows largely that of the electron density being as peaked as

the electron density at high ECRH fraction, or less peaked than the electron density at high NBI fraction. Excellent database has been assembled, but no He particle transport models have been suggested for predicting the He density profiles in these discharges.

Generally, the number of the transport model validation studies performed for He plasmas is rather limited compared to D plasmas. The empirical Bohm-gyroBohm (BgB) model for thermal electron transport [11] has been validated in the Tore Supra RF-heated L-mode He discharges showing a good agreement between the simulated and measured electron temperature ( $T_e$ ) [12]. The theory-based Multi-Mode Model (MMM) [13] has been also validated in the same L-mode discharges, predicting reasonably well the electron and ion ( $T_i$ ) temperatures and the main He ion ( $n_{He}$ ) and carbon (C) impurity densities in the self-consistent simulations of these four quantities [14]. However, the predictive capabilities of existing transport models in the He H-mode confinement regime remain unexplored. Consequently, various assumptions on the He particle transport and confinement have been used in the predictive modelling of burning plasmas for the estimation of He ash accumulation. The simplest assumptions include the fixed ad-hoc He density profiles or  $\tau_{He}/\tau_E$  ratio (here  $\tau_{He}$  is the global He particle confinement time), arbitrary values for the He particle diffusion coefficient  $D_{He}$  and convective velocity  $V_{He}$  [15] or arbitrary ratios of He diffusion coefficient to thermal ion ( $\chi_i$ ) or electron ( $\chi_e$ ) diffusivity (for example,  $D_{He}/\chi_i = 0.5$ ,  $V_{He} = 0$  [16] or  $D_{He}/\chi_e = (0.2 - 0.35$  and arbitrary  $V_{He}$  value [17, 18]). It was also shown that the performance of burning plasma in the simulated ITER and DEMO H-mode scenarios (for example, the fusion power [17, 18] or the duration of the sawtooth stable operation dependent on the plasma effective charge ( $Z_{eff}$ ) [12]) is highly sensitive to the assumptions on He particle transport.

In this brief communication, the particle and thermal transport in JET C wall (CW) and ITER-like wall (ILW, a tungsten divertor and Be main chamber) He H-mode discharges is analysed with the goal to validate the simple computationally fast empirical BgB transport model



frequently used for the modelling of thermal transport in reactor scenarios and in the real-time control codes. This model for thermal electron and ion diffusivities, well validated in D plasmas, is used here as a D reference for the comparison with the thermal transport in He plasma. As the unique BgB model for particle transport coefficients has not been developed and validated yet (different versions of the BgB model are used in various modelling works [19, 20]) a constant ratio of He diffusion coefficient to thermal diffusivity  $D_{He}/\chi_e$  in combination with the model for convective velocity suggested in [20] is assumed here and this ratio is determined in predictive modelling of selected discharges. To validate the modelling approach where the BgB particle transport has been tuned to match the GLF23-computed transport predicting important anomalous particle pinch [21] the GLF23 model [22] is tested here in the temperature and density simulations in the mixed H-He discharge. This theory-based model is used also to investigate an impact of He concentration on thermal confinement. In the following, the JET discharges selected for modelling are described in section II, the simulation assumptions and models applied are given in section III and the modelling results are presented in section IV. The results of the application of the JET He particle transport model to the future devices – ARC and EU-DEMO – for the estimation of the He ash accumulation in the burn phase and its impact on the fusion power production are shown in section V. The conclusions follow in section VI.

## **II. Selected discharges and diagnostics used for the transport model validation**

Three JET H-mode He discharges and one mixed H-He discharge performed at low triangularity (0.22 - 0.3), similar NBI power ( $P_{nbi} = 10 - 12$  MW) and edge safety factor ( $q_{95} = 2.9 - 3$ ) in the low-to-medium density range are selected for modelling. Two of these discharges executed during the 2001 JET He campaign in the CW configuration are performed at different toroidal magnetic field  $B_{tor}$  and plasma current  $I_{pl}$ . Two recent ILW discharges with a low  $B_{tor}$

and  $I_{pl}$  [8] are selected for the comparison of the He plasma performance in CW and ILW configurations and for the extension of the validation domain from a pure He plasma to a plasma with a reduced He content. Core He NBI fuelling has been used in all discharges. No He gas puff has been applied in the CW discharges at the time of interest selected during the stationary NBI power flat top phase, while the He and H gas fuelling has been used in the ILW He and mixed H-He plasma correspondingly. The main plasma parameters for the selected discharges at the time of interest are given in Table 1.

The data from the following diagnostics have been used for this study. The electron temperature in discharge 54182 has been measured using an ECE and a Thomson scattering (TS) diagnostics while the TS measurements only have been used in discharge 54185. The density in these two discharges has been measured with the same TS system combining the core and edge data. The more advanced high resolution TS (HRTS) system has been used for the density and temperature measurements in two recent ILW discharges. In the absence of the ion temperature measurements for the ILW discharges and CW discharge 54182 the diamagnetic energy has been used for the validation of the simulated thermal ion confinement. The measurements of the total bulk radiation have been obtained by using the horizontal channel of bolometer camera for the CW discharges while the tomographic reconstruction of the multi-chord bolometer measurements has been performed for two ILW discharges. The bremsstrahlung measurements of  $Z_{eff}$  have been used, with a radially flat  $Z_{eff}$  profile assumed in simulations. Low Nickel (Ni) concentration has been found in ILW discharges by using VUV emission spectroscopy [23] ( $n_{Ni} = (2 - 3.2)10^{-5}$ ). Consequently, Beryllium (Be) has been considered as a main impurity in the simulations of discharges 101445 and 101448, while the C impurity has been used in simulations of two other discharges. Divertor diagnostics for neutral gas analysis is used for the measurements of He fraction.

### III. Simulation model

The He thermal and particle transport models have been validated in the self-consistent simulations of current diffusion, equilibrium, electron and ion temperatures and main ion densities. Two separate particle balance equations for H and He species have been used in case of H-He plasma. The expression for  $Z_{eff}$  and the quasi-neutrality constraint have been used to compute the Be and electron densities. The NBI heating, fuelling, current drive and fast ion density profiles have been simulated with the PENCIL code [24]. In pure He plasmas the He influx through the separatrix (which may be caused by He recycling) has been adjusted to maintain the electron volume averaged density  $\langle n_e \rangle$  close to its measured value, while the feedback control to the H gas puff has been applied in the mixed species case for the same purpose. In the latter case, the He gas influx through the separatrix has also been adjusted to reproduce the measured He fraction in simulations.

The thermal electron and ion diffusivities include the core anomalous transport described by the BgB model ( $\chi_{e(i),BgB}$ ) validated in D plasmas [11], neoclassical transport ( $\chi_{e(i),neocl}$ ) and the edge diffusivity ( $\chi_{e(i),edge}$ ) applied in the pedestal region only ( $\rho \geq \rho_{ped}$ ):

$$\chi_{e(i)} = \chi_{e(i),BgB}(\rho < \rho_{ped}) + \chi_{e(i),neocl} + \chi_{e(i),edge}(\rho \geq \rho_{ped}) \quad (1)$$

Here

$$\begin{aligned} \chi_{e,BgB} &= \begin{cases} \chi_{Bohm}^L & \text{in L - mode confinement regime} \\ \chi_{Bohm}^H & \text{in H - mode confinement regime} \end{cases} + \chi_{gyroBohm}, \\ \chi_{i,BgB} &= 2\chi_{Bohm}^H + 0.5\chi_{gyroBohm}, \\ \chi_{Bohm}^H &= 0.32\chi_{Bohm}^L \frac{T_e(\rho = 0.74) - T_e(\rho = 0.85)}{T_e(\rho = 0.85)} \\ \chi_{Bohm}^L &= 0.33 \frac{T_e}{B_{tor}} \left( \frac{a}{L_p} \right) q^2 \\ \chi_{gyroBohm} &= 0.32 \frac{\sqrt{A_i} T_e^{3/2}}{B_{tor}^2 Z_i L_{Te}} \end{aligned} \quad (2)$$

$a/L_p = a \nabla p/p$  ( $a$  is the minor radius and  $p$  is the thermal pressure),  $L_{Te} = T_e/\nabla T_e$  (in m),  $q$  is the safety factor,  $\rho$  is the square root of toroidal magnetic flux,  $0 < \rho < \rho_{ped}$  is the region of application of the BgB model in the H-mode regime,  $A_i$  and  $Z_i$  are the mass and charge numbers of main ions. The thermal diffusivities and  $B_{tor}$  in Eqs. (1, 2) are given in  $m^2/s$  and T correspondingly. Although the parametric dependencies in the BgB model have been determined in a purely empirical manner by predicting the temperature profiles in different tokamaks as accurately as possible [11], they include some theory-based effects, such as the increase of anomalous transport with the increase of the temperature and pressure gradients or the  $q^2$  dependence of transport driven by the drift-resistive ballooning mode [25]. The Bohm-like terms  $\chi_{Bohm}^H$  and  $\chi_{Bohm}^L$  are the dominant terms in the H- and L-mode regimes correspondingly, while the gyroBohm term  $\chi_{gyroBohm}$  becomes important when the Bohm-like transport is reduced due to a turbulence stabilisation by magnetic or  $ExB$  shear (for example, in advanced scenarios). The examples of validated magnetic and  $ExB$  shear dependencies can be found in [13, 20, 26] (not applicable here and not included in Eq. (2)).

Similarly to the approach applied in Ref. 20 the following form of the particle transport coefficients is assumed here:

$$D_j = D_{BgB}(\rho < \rho_{ped}) + D_{j,neocl} + D_{j,edge}(\rho \geq \rho_{ped}) \quad (3)$$

$$V_j = V_{j,an} + V_{neo}, \quad V_{an} = 0.015(\omega_{ce}/\omega_{pe})^2 D_{BgB} \nabla q,$$

where  $j$  indicates the plasma species (He or H),  $D_{BgB} = C\chi_{e,BgB}$ ,  $C$  is the constant coefficient to be determined in section IV(a),  $\omega_{ce}$  and  $\omega_{pe}$  are the electron cyclotron and electron plasma frequency correspondingly. The neoclassical transport coefficients  $\chi_{e,neocl}$ ,  $\chi_{i,neocl}$ ,  $D_{j,neocl}$  and  $V_{j,neo}$  are simulated with NCLASS [27] and the edge thermal and particle diffusion coefficients  $\chi_{e(i),edge}$  and  $D_{j,edge}$  are adjusted to match the electron density and temperature at  $\rho_{ped} = 0.85$ . The anomalous particle pinch  $V_{an}$  introduced in [20] to describe the density evolution in the discharges with strong reversed magnetic shear is negligible in considered JET discharges, the

ratio  $V_{an}/V_{He,neo}$  is below 3% within mid-radius and it gradually increases towards the edge reaching 8% at the pedestal. With this set of transport models, the possibility to predict the density profiles in all selected discharges by using the same coefficient  $C$  is explored.

The GLF23 model has been applied to the mixed H-He discharge only. Hydrogen has been treated as the main plasma species in these simulations while He was considered as an impurity (along with Be). This model applied in the core plasma region ( $0 < \rho < \rho_{ped}$ ) has been complemented with the neoclassical and edge transport coefficients similarly to the BgB case. All simulations presented here have been performed with the ASTRA code [28, 29].

#### IV. Validation of transport models

##### (a) *Bohm-gyroBohm model*

The temperature simulations have been performed with the measured density at a first step to check if the core thermal transport in He plasma can be predicted with the D BgB reference model,  $\chi_{e(i),BgB}(D)$ . Strongly overpredicted  $T_e$  has been found in all four discharges. An example of the disagreement between the simulated and measured  $T_e$  is shown in Fig. 1 for discharge 54182. Even in the case of a better core confinement experimentally achieved at high toroidal magnetic field the measured electron temperature is still below the one simulated with the H-mode BgB model, and it appears to be closer to the  $T_e$  predicted with the L-mode BgB version. Subsequent adaptation of thermal BgB model to He plasma has been done for its H-mode version taking into account that the H-mode has been achieved in all simulated discharges (i.e. the Edge Localised Modes (ELMs) and a moderate  $T_e$  pedestal on the temperature profiles have been observed). At the next step, the H-mode thermal diffusivity has been rescaled by introducing the constant coefficient in front of the BgB term in Eq. (1) and varying its value until a reasonable agreement with the measured  $T_e$  is achieved for discharge 54182. The most accurate prediction has been obtained by increasing the BgB thermal diffusivity by factor 6

(i.e.  $\chi_{e(i),BgB}(He) = 6\chi_{e(i),BgB}(D)$ ). With such a relatively large factor, the He thermal diffusivity computed in predictive modelling exceeds the D BgB reference by factor 2 only due to the stiffness of the BgB model. Using this heat calibration factor for the He thermal diffusivity the particle calibration factor  $C$  has been determined in the self-consistent temperatures and density simulations, with the most accurate prediction for density obtained with  $C = 0.75$ . Figures 2 and 3 show the variation of density peaking with the change of this coefficient (Fig.2) and the density profiles obtained with three different  $C$  values (Fig. 3, top left panel). The sensitivity of the density peaking to the choice of diffusion coefficient  $C$  is obviously different in cases of the peaked and flat  $n_e$  profiles showing that in the absence of convective particle losses or at low convective velocity (that is the case of the BgB model where the neoclassical convection is used) the particle diffusion coefficient can be determined relatively accurately only in the peaked  $n_e$  case. The uncertainty of the  $C$  value ( $C = 0.5 - 1.1$ ) shown by dashed lines in Fig. 2 is determined by the error bars of the density measurements, the density profiles simulated with  $C = 0.5$  and  $1.1$  are still within the error bars of the TS data (Fig. 3, top left panel, dashed curves). Based on the model calibration performed for discharge 54182 the anomalous transport coefficients  $\chi_{e(i),BgB}(He) = 6\chi_{e(i),BgB}(D)$  and  $D_{BgB} = 0.75\chi_{e,BgB}(He)$  are applied in the temperature and density simulations of three other discharges.

The simulations of the CW discharges with the BgB model recalibrated for He plasma are presented in Fig. 3. The density and electron temperature profiles are reasonably accurately predicted in the region  $\rho_\psi = 0.3 - 0.85$  (here  $\rho_\psi$  is the square root of poloidal magnetic flux  $\psi$ ), while the electron and ion temperatures as well as the density in discharge 54185 are over-predicted in the core region  $\rho_\psi < 0.3$  where thermal and particle confinement may be affected by the frequent sawtooth oscillations observed in these discharges. Figure 3 illustrates also a strong impact of magnetic field on He thermal and particle transport well reproduced with the BgB model: much higher  $T_e$  and  $n_e$  are achieved with the same heating and core He fuelling

sources when the magnetic field is increased by factor three. The He diffusion coefficient in the core plasma region is reduced by factor 2 at high  $B_{tor}$ .

The contributions of central He particle source and inward convection to the density peaking in CW discharges has been investigated by repeating the simulations shown in Fig. 3 either without the He NBI fuelling or with zero inward convection (Fig. 4). The same He transport coefficients have been used in the pedestal region in simulations with zero convective velocity as in the reference case (Fig. 3), but  $D_{He,edge}$  has been reduced in the case of zero NBI fuelling to match (i.e. avoid a reduction of) the pedestal density. While the effect of the neoclassical (and tiny anomalous) pinch appears to be negligible, a strong impact of the central source on the density profile has been found in discharge 54182. The dependence of the density peaking on the central He fuelling is less pronounced in the low-density discharge 54185 where the peaked fast ion density and C impurity profiles produce an important contribution to the density peaking.

The simulations of the ILW He and H-He discharges are shown in Figs. 5 and 6. These discharges have been performed at higher  $B_{tor}$  and  $I_{pl}$  and lower density compared to discharge 54185. The radiative power is much larger in the ILW discharges than in the CW discharges ( $P_{rad} = 0.45 - 0.66$  MW in the CW discharges and  $P_{rad} = 2.7 - 2.8$  MW in the ILW discharges), this high radiative power appears to be close to the electron heating by NBI. The fast ion content is also different in the CW and ILW discharges, being much lower in the latter case that may be explained by a lower energy of injected neutrals. Thus, with the inclusion of the ILW discharges the tested parameter space is extended towards the lower total electron heating (due to high radiation) and the lower fast ion fraction.

The modelling of the ILW discharges shows that the density is predicted reasonably well while the electron temperature is slightly overpredicted in discharge 101448, with a more visible difference between the measured and simulated  $T_e$  in discharge 101445. However, this  $T_e$

overestimation weakly affects the density prediction as shown by the simulation case performed with the artificially increased thermal diffusivities (but without corresponding artificial increase of the particle calibration factor  $C$ ) and reduced electron temperature (Figs 5 and 6, dashed curves).

**(b) GLF23 model**

Since the density of H ions is dominant in discharge 101448, this discharge has been simulated with the GLF23 model designed for hydrogenic species to obtain some insight on the transport physics. This model has been applied in a way suggested in Ref. 14, i.e. by treating Helium as an impurity with the full impurity dynamics computed while considering Hydrogen as the main plasma species. Zero toroidal rotation velocity ( $V_{tor}$ ) has been assumed in these simulations since  $V_{tor}$  was not measured, but the contribution of the neoclassical poloidal and diamagnetic rotation velocities to the  $ExB$  shear ( $s_{ExB}$ ) has been taken into account. The impact of the  $ExB$  shear stabilisation has been tested under assumptions of the  $s_{ExB}$  value computed by ASTRA as described above, the  $ExB$  shearing rate computed internally within the GLF23 model and zero  $ExB$  shear. The effect of the  $ExB$  shear stabilisation is found to be negligible at  $\rho \geq 0.25$  in these simulations. Some difference between the simulations performed with and without the  $ExB$  shear stabilisation appears in the core region only ( $\rho < 0.25$ ) where the central electron and ion temperatures decrease by 13% and 18% correspondingly in simulations with  $s_{ExB} = 0$ . The density and temperature profiles obtained in the simulations with the GLF23 model are shown in Fig. 7 (solid curves). The density peaking is overestimated when the He concentration is close to 25% (i.e. with  $n_H/n_e \cong 0.5$  as reported in [8]) due to a strong inward anomalous pinch in the broad core plasma region ( $\rho_\psi < 0.6$ ). Electron temperature is predicted reasonably accurately outside the mid-radius, while the core  $T_e$  is slightly underestimated. This figure illustrates also an impact of He concentration on the temperature and density profiles obtained



in simulations where the He influx through the separatrix has been reduced while maintaining the same volume averaged density via the H gas puff control (dashed and dotted curves). The anomalous pinch reduces with the reduction of He concentration and consequently  $n_H$  is almost flat with  $\sim 8\%$  of He (Fig. 7, dotted curves). The inclusion of full He dynamics in the GLF23 model appears to be important: the simulations with the simple dilution model for He (i.e. without using the equation for He impurity in the eigenvalue solver, but taking He into account in the  $Z_{eff}$  estimation) performed for the reference case shown by solid curves in Fig. 7 (i.e. with  $n_H/n_e \cong 0.5$ ) predict a flat density profile with 20% of He concentration. An impact of the central fuelling on density peaking simulated with the GLF23 model has been tested for the reference case with  $n_H/n_e \cong 0.5$ . Figure 8 shows the comparison of this reference case with the simulations where the core He fuelling has been fully replaced with the He gas puff, adjusted to maintain the same He concentration (Fig. 8, dashed curves). The NBI particle source only has been removed in this simulation, while the NBI heating has been maintained. The inward convective velocity and electron and He density peaking strongly decrease in the absence of core particle source, but the anomalous convective velocity is still well above its neoclassical value in the plasma core maintaining some hydrogen and electron density peaking. The temperature profiles are resilient and weakly affected by the change of density.

## **V. Impact of the He ash accumulation on the fusion power production in ARC and EU-DEMO**

Strong beneficial effect of toroidal magnetic field on the He particle confinement found in JET discharges suggest that the He ash accumulation may substantially limit the fusion power production in the tokamak-reactor facilities with high  $B_{tor}$ . One of such facilities - a future compact tokamak-reactor ARC [30] where the high temperature superconductors will allow the operation at  $B_{tor} = 9.2$  T is used here for estimating this effect. The ASTRA simulations of

the ARC steady state burn phase performed here include the solution of the continuity equation for thermalised He particles used with the He transport coefficients validated in JET, the Grad-Shafranov equilibrium equation and the current diffusion equation with the NCLASS module computing the resistivity and the bootstrap (BS) current. The ARC global parameters, the stationary temperature and density profiles as well as the Lower Hybrid (LH) and Fast Wave (FW) current density profiles given in [30] (Table 1 and Figs 5 and 12) are used in these simulations. The thermal He particle source is determined by the slowing down of fast  $\alpha$ -particles born in the D-T reaction and by the He influx through the separatrix caused by recycling (this approach is described in [16]). The Gaussian radial profile of the recycling source peaked at the plasma boundary with the width of 10% of the plasma radius is assumed. The pumping efficiency  $A = \Gamma_{in}/\Gamma_{out}$  (here  $\Gamma_{in(out)}$  is the He particle influx (outflux) through the separatrix into the plasma) and the He pedestal diffusion coefficient  $D_{He,edge}$  are the free parameters of these simulations and their impact on the He ash accumulation is assessed below. The magnetic configuration obtained in the ASTRA simulations by using the fixed kinetic, FWCD and LHCD profiles and the bootstrap current density computed by NCLASS is characterised by the broad core region with an elevated nearly flat  $q$ -profile with  $q_{min} \sim 2$  ( $q_{min}$  is the minimum safety factor). A relatively low He ash concentration ( $N_{He}/N_e = 0.006$ , here  $N_{He(e)}$  is the total number of He (electron) particles in the plasma volume) producing a small impact on the fusion power ( $P_{fus} = 505$  MW in this case and 515 MW in the absence of the He ash) has been obtained in this magnetic equilibria by using the He diffusion coefficient  $D_{BgB} = 0.75\chi_{e,BgB}(He)$  validated in JET plasma and the pedestal diffusion coefficient  $D_{He,edge} = 0.21$  m<sup>2</sup>/s used in the JET discharge with the highest magnetic field (54182,  $B_{tor} = 3$  T) to predict the pedestal density. Such a low He ash accumulation obtained at high magnetic field is caused by the counteracting contributions of high  $B_{tor}$  and elevated  $q$ -profile to the He particle transport ( $D_{BgB} \sim q^2/B_{tor}$ , see Eq.(1-3)). The effect of the plasma dilution by He ash on fusion power

remains small in the range of the wall pumping efficiency  $A = 0 - 0.6$  and within the uncertainty in the ratio  $D_{BgB}/\chi_{e,BgB}(He) = 0.5 - 1.1$  estimated in the JET high  $B_{tor}$  discharge: the variation of the fusion power is within 6 MW in these parameter space. However, the He concentration strongly increases with the reduction of the He pedestal diffusion coefficient below  $0.05 \text{ m}^2/\text{s}$  and its impact on the fusion power production becomes important (Fig. 9). The self-consistent simulations of the He density and the thermal energy balance would be desirable at low  $D_{He,edge}$  values for a proper estimation of the He ash effect.

The  $D_{He}/\chi_e$  ratio found in the analysed JET discharges appears to be more optimistic than the one used in the ITER and EU-DEMO simulations in Refs. 17 and 18. Using the results obtained in [18] with two different  $D_{He}/\chi_e$  values (0.2 and 0.35), a simple linear extrapolation can be made to estimate an impact of the higher  $D_{He}/\chi_e$  ratio on the fusion power in the H-mode EU-DEMO scenario. Taking into account that the increase of the  $D_{He}/\chi_e$  ratio by 75% (i.e. from 0.2 to 0.35) leads to the 20% increase in the fusion yield in the absence of Ar seeding (Ref. 18, Fig.4), further increase of this ratio from 0.35 to 0.75 may lead to the increase of fusion  $Q$  value up to 78 due to a reduced He ash content.

## VI. Summary and conclusions

Two models for He particle and thermal transport (BgB and GLF23) have been tested in the self-consistent predictive temperature and density (with one or two main species) simulations of JET NBI-heated H-mode He and H-He discharges, with a purpose to suggest a validated model for predicting the core He ash content in burning plasma. Two selected discharges represent the scan in the toroidal magnetic field and plasma current performed at fixed  $q_{95} = 2.9-3$  and NBI heating power in the CW configuration. Two additional JET ILW discharges are added to extend the validation parameter space: one He discharge at high density with strong impurity radiation at relatively low magnetic field; and an H-He discharge with  $n_{He}/n_e \sim$

0.25, to test the impact of the He fraction on particle and energy confinement in conditions closer to the more modest He fraction expected in burning plasmas.

The main emphasis is made in this work on the validation and adaptation of the computationally fast BgB model as it is frequently used in the modelling of entire reactor scenario and implemented in the plasma control codes. This model, well validated for the thermal transport in D plasmas, has not been validated in He H-mode regimes. The modelling performed here shows that the D BgB model strongly overpredicts the temperatures in Helium. This is qualitatively consistent with the number of experiments on various tokamaks reporting a lower global energy confinement in He plasmas compared to the D ones [1-7]. Following this result obtained for four JET discharges the “Helium” version of the BgB model has been proposed and tested. This BgB version includes the calibration coefficient added to the thermal D BgB model ( $\chi_{e(i),BgB}(He) = 6\chi_{e(i),BgB}(D)$ ) and the anomalous He particle diffusion coefficient proportional to thermal electron diffusivity  $D_{BgB} = 0.75\chi_{e,BgB}(He)$ . The He density profiles are accurately predicted with this model in the low-to-medium density range and broad range of  $B_{tor} = 1 - 3$  T showing a beneficial effect of magnetic field not only on the thermal, but also on the He particle confinement. The density peaking is determined by central fuelling in this approach.

Some insight on the transport physics has been gained by using the theory-based GLF23 transport model computing the transport of hydrogenic ions as a main species. This model has been applied to the mixed H-He plasma to investigate in particular an impact of anomalous particle pinch on density peaking and its dependence on He concentration. In difference to the BgB model, the GLF23 predicts electron temperature much more accurately in this ITG-dominant plasma, still slightly underpredicting it in the core region. The density peaking is overpredicted due to a strong anomalous particle pinch when the He fraction is close to 25%. It should be mentioned that the mixed H-He discharges at JET are not sufficiently well

diagnosed to validate the He particle transport models accurately as the He density profile is not measured, the H concentration is measured at the plasma edge only and the neutron emission which could help to validate the He density profile is not produced in H plasma. Reducing the assumed He concentration in the core to 12-15%, the electron density peaking can be reasonably reproduced with the GLF23 model. Electron temperature profiles computed both with the GLF23 and BgB models display some stiffness – strong density reduction in the core region obtained in the absence of central fuelling weakly affects the temperature profiles in discharges 54182 and 101448.

The strong increase of the He particle confinement with the toroidal magnetic field found in the JET discharges raises a concern about the He ash accumulation in the future high  $B_{tor}$  devices. Taking ARC [30] as an example of the tokamak-reactor with high magnetic field, the effect of the He ash accumulation on the fusion power production has been simulated by using the He particle transport model validated in JET. Low He ash accumulation weakly affecting the fusion power production in a broad parameter space has been found in these simulations due to the elevated flat or marginally reversed  $q$ -profile in the core plasma region obtained with the central FWCD, the off-axis LHCD and BS current density. In such magnetic configuration the reduction of the He particle transport caused by the high magnetic field is compensated by its  $q^2$ -dependence increasing the He diffusion. However, the presumably improved particle confinement in this hybrid-like magnetic configuration may change this prediction.

The H-mode EU-DEMO scenario with moderate  $B_{tor}$  (5.9 T) and monotonic  $q$ -profile with  $q_0 \sim 1$  could potentially exhibit a good He particle confinement. But the self-consistent core-divertor simulations performed with the COREDIV code by using even lower  $D_{He}/\chi_e$  ratios than the one found in JET discharges show that a sufficiently high fusion yield ( $Q_{fus} \sim 37$ ) can be achieved with  $D_{He}/\chi_e = 0.2$  in the absence of impurity seeding [18]. Indeed, the increase of the He concentration in the core plasma region occurring with the reduction of the He diffusion

leads to the reduction of the fusion power and consequently the reduction of the heat flux crossing the separatrix and deposited at the divertor plates. This causes the reduction of the divertor temperature and the tungsten (W) sputtering at the divertor plates and consequently the reduction of the W influx and radiation in the plasma core. This non-linear coupling between core and divertor in presence of strongly radiating impurity (W) makes the fusion power production more resilient with respect to the change of He concentration as the reduced W radiation counteracts the effect of plasma dilution by He ash.

### **Acknowledgments**

This work has been carried out within the framework of the EUROfusion Consortium, funded by the European Union via the Euratom Research and Training Programme (Grant Agreement No 101052200 – EUROfusion) and from the EPSRC (grant number EP/W006839/1). The views and opinions expressed are however those of the authors only and do not necessarily reflect those of the European Union or the European Commission. Neither the European Union nor the European Commission can be held responsible for them. This scientific paper has been published as part of the international project co-financed by the Polish Ministry of Science and Higher Education within the programme called “PMW”.

Table 1. Parameters of JET He discharges selected for modelling

	Wall type	Toroidal magnetic field, T	Plasma current, MA	NBI power, MW	Volume averaged density/ $10^{19}$ , $\text{m}^{-3}$	He fraction
54182	CW	3.2	3.2	10.7	3.24	0.94
54185	CW	1	1	10	2	0.85
101445	ILW	1.3	1.26	10.8	3.6	0.95
101448	ILW	1.3	1.26	12.3	3.7	0.25

## References

1. D. P. Schissel, et al., Nucl. Fusion **29** (1989) 185
2. D. L. Hillis, et al., Plasma Phys. Control. Fusion **36** (1994) A171
3. F. Ryter, et al., Nucl. Fusion **49** (2009) 062003
4. C. E. Kessel, et al., Nucl. Fusion **58** (2018) 056007
5. B. Zhang, et al., Nucl. Fusion **60** (2020) 092001
6. D. C. McDonald, et al., Plasma Phys. Control. Fusion **46** (2004) 519
7. D. C. McDonald, et al., IAEA FEC 2010 p EXC/2-4Rb ([www-pub.iaea.org/mtcd/meetings/PDFplus/2010/cn180/cn180\\_papers/exc\\_2-4rb.pdf](http://www-pub.iaea.org/mtcd/meetings/PDFplus/2010/cn180/cn180_papers/exc_2-4rb.pdf))
8. M. Maslov, et al., 49<sup>th</sup> EPS Conf. on Contr. Fusion and Plasma Physics, Bordeaux, 3 - 7 July 2023
9. P. Manas, et al., Nucl. Fusion **59** (2019) 014002
10. A. Kappatou, et al., Nucl. Fusion **59** (2019) 056014
11. M. Erba, et al., Plasma Phys. Control. Fusion **39** (1997) 261; see also A Taroni, et al., Plasma Phys. Control. Fusion **36** (1994) 1629
12. I. Voitsekhovitch, et al., Nucl. Fusion **37** (1997) 1715
13. G. Bateman, et al., Phys. Plasmas **5** (1998) 1793
14. I. Voitsekhovitch, et al., Phys. Plasmas, **9** (2002) 4241
15. R. V. Budny, et al., Nucl. Fusion **48** (2008) 075005
16. G. Kamelander, et al., Fus. Science and Technology, **39** (2001) N° 2
17. I. Ivanova-Stanik, et al., Fusion Eng. Des. **109-111** (2016) 342-346
18. I. Ivanova-Stanik, et al., Fusion Eng. Des. **146** (2019) 2021-2025
19. L. Garzotti, et al., Nucl. Fusion **43** (2003) 1829



20. I. Voitsekhovitch, et al., 26<sup>th</sup> EPS Conf. on Contr. Fusion and Plasma Physics, Maastricht, 14 - 18 June 1999, ECA Vol.23J (1999) 957 - 960
21. S. H. Kim, et al., Nucl. Fusion **57** (2017) 086021
22. R. E. Waltz, et al., Phys. Plasmas **4** (1997) 2482
23. A. Czarnecka, et al., Plasma Phys. Control. Fusion **53** (2011) 035009
24. G Corrigan, et al., Report JET-R(91)14, JET Joint Undertaking, 1992
25. J. F. Drake, et al., Phys. Rev. Letters **77** (1996) 494
26. I. Voitsekhovitch, et al., Phys. Plasmas **6** (1999) 4229
27. W. A. Houlberg, et al., Phys. Plasmas **4** (1997) 3230
28. G. Pereverzev, P. N. Yushmanov, "ASTRA Automated System of TRansport Analysis in a Tokamak", Report of the Max-Planck-Institut für Plasmaphysik, IPP 5/42 (Garching Germany, 1991)
29. E. Fable, et al., Nucl. Fusion **53** (2013) 033002
30. B.N. Sorbom et al., Fusion Eng. Des. **100** (2015) 378-405

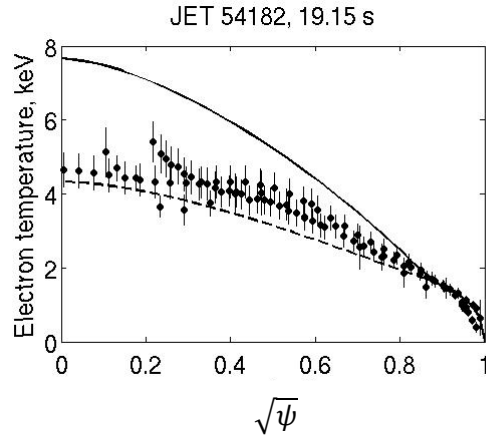


*Fig. 1. CW discharge 54182: simulated electron temperature with the L-mode (dashed curve) and H-mode (solid curve) BgB model validated in D plasma. Measured density profile is used in these simulations. The TS and ECE measurements with error bars are shown by symbols.*

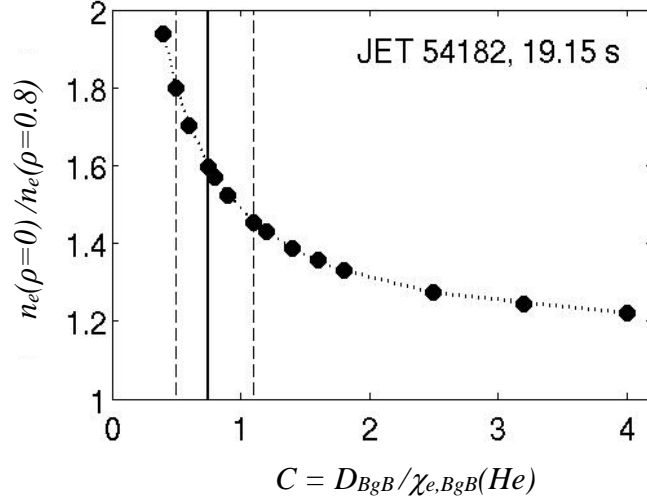


Fig. 2. CW discharge 54182: density peaking as a function of the  $D_{BgB}/\chi_{e,BgB}(He)$  ratio obtained in the self-consistent temperature and density simulations. The convective velocity is computed following Eq. (3). Solid and dashed lines indicate the  $D_{BgB}/\chi_{e,BgB}(He)$  ratios used for the density predictions shown in Fig.3 (top left panel). The density peaking at large  $D_{He}/\chi_e$  ratio is determined by the fast ion and C impurity densities.

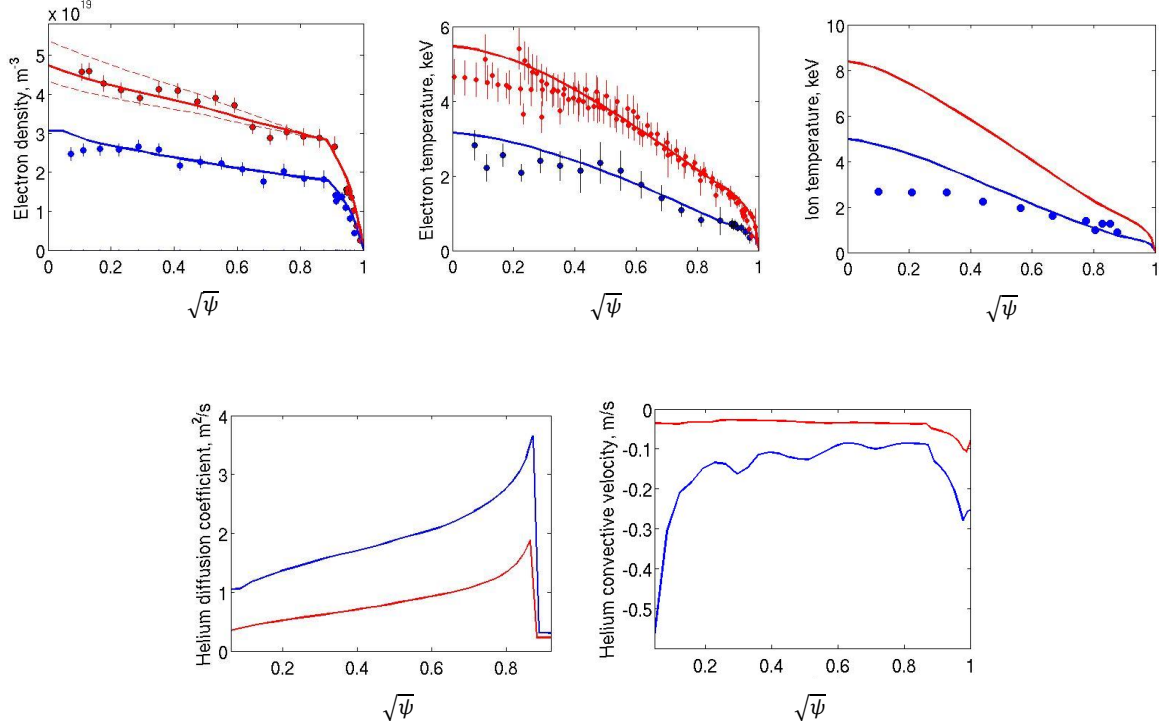
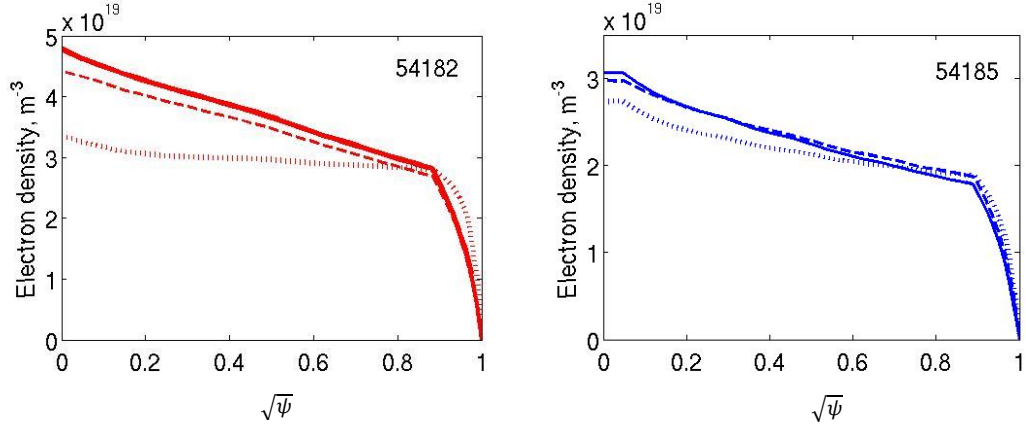
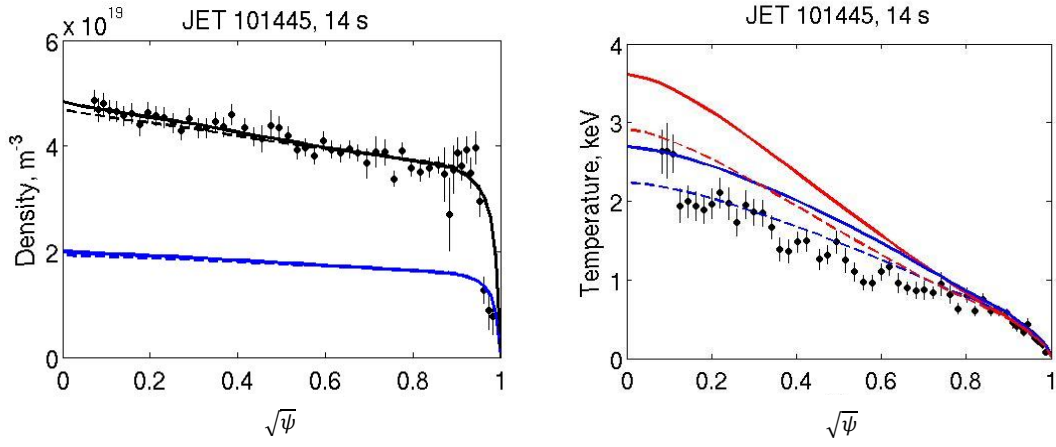


Fig. 3. Electron density (top left panel), electron (top middle panel) and ion (top right panel) temperatures, He diffusion coefficient (bottom left panel) and convective velocity (bottom right panel,  $V_{\text{He}} < 0$  indicates inward convection) obtained in simulations with recalibrated  $H$ -mode BgB model ( $\chi_{e(i),\text{BgB}}(\text{He}) = 6\chi_{e(i),\text{BgB}}(D)$ ,  $D_{\text{BgB}} = 0.75\chi_{e,\text{BgB}}(\text{He})$ ) in JET CW He discharges 54182 (red) and 54185 (blue). The measured temperatures and density profiles with error bars are shown by symbols. The red dashed curves in the top left panel show the simulations performed with  $D_{\text{BgB}}/\chi_{e,\text{BgB}}(\text{He}) = 0.5$  and  $1.1$ .



*Fig. 4. Electron density in CW discharges 54182 (left panel) and 54185 (right panel) obtained in simulations with zero convective velocity (dashed curves) and zero NBI fuelling (dotted curves). Solid curves show the reference cases presented in Fig. 3.*



*Fig. 5. ILW He discharge 101445: Helium (blue) and electron (black) densities (left panel) and electron (blue) and ion (red) temperatures (right panel) obtained in simulations with the recalibrated BgB model (solid curves). Dashed curves show the variation of the density with the change of electron and ion temperatures obtained by increasing the thermal diffusivities by factor 2, but keeping the same  $D_{\text{BgB}}/\chi_{e,\text{BgB}}(\text{He})$  ratio. Symbols show the HRTS measurements with error bars.*

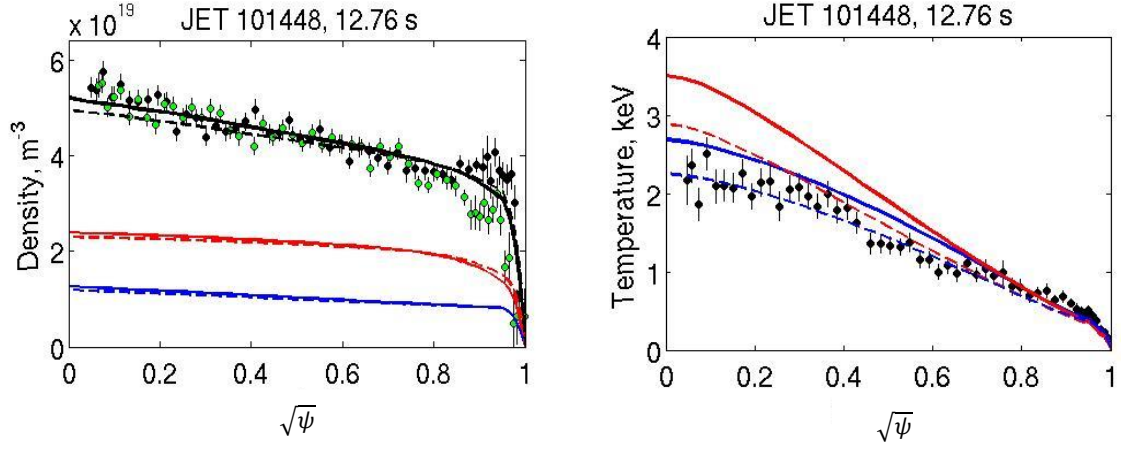
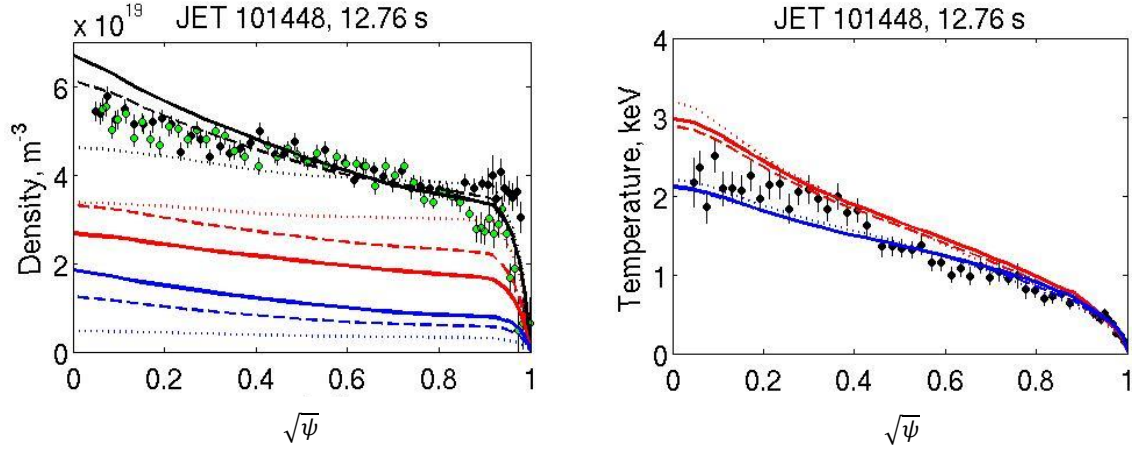


Fig. 6. ILW H-He discharge 101448: electron (black), He (blue) and H (red) densities (left panel) and electron (blue) and ion (red) temperatures (right panel) obtained in simulations with the recalibrated BgB model (solid curves). Dashed curves show the variation of the density prediction with the change of electron and ion temperatures obtained by increasing the thermal diffusivities by factor 2. Symbols show the HRTS measurements with the error bars. Black circles on the left panel show the density profile measured at 12.76 s (before the ELM crash), green circles show the density profile measured after the ELM crash.



*Fig. 7. ILW H-He discharge 101448: electron (black), He (blue) and H (red) densities (left panel) and electron (blue) and ion (red) temperatures (right panel) obtained in simulations with the GLF23 model by using different He concentration: 78% H & 8.7% He (dotted), 61.7% H and 17% He (dashed), 47.6% H and 24.4 % He (solid). Symbols show the same measurements as in Fig. 6.*



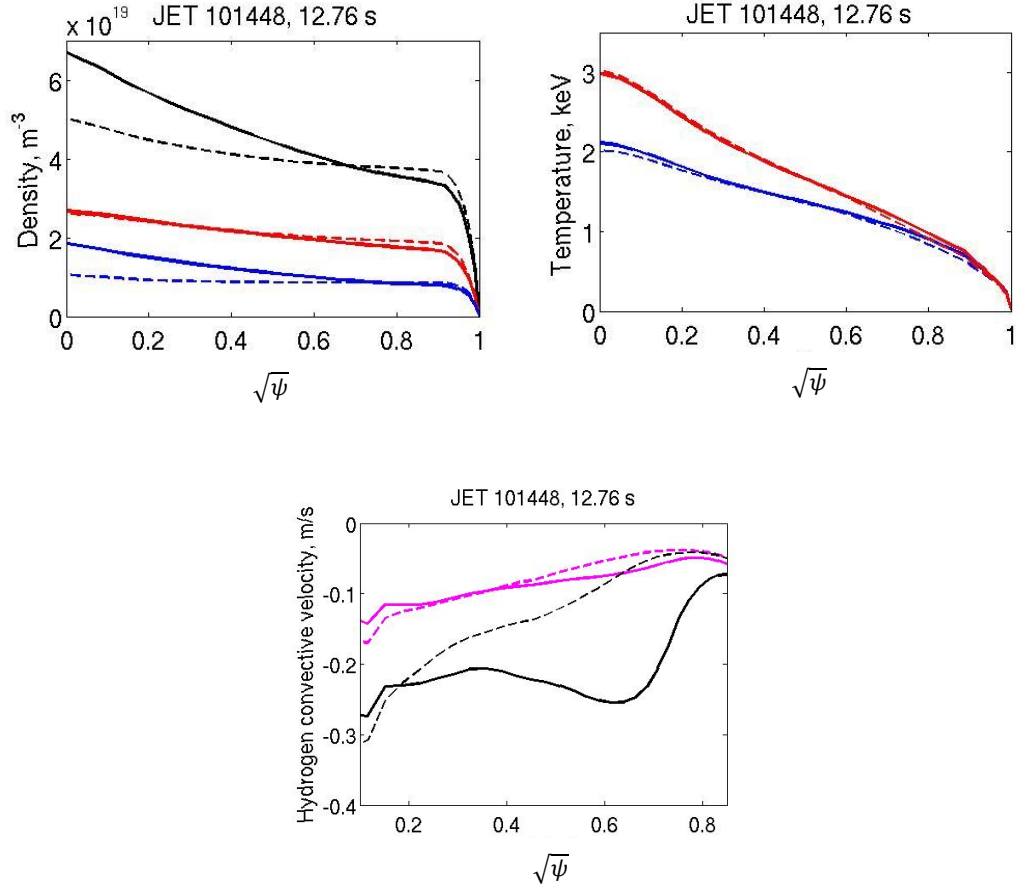
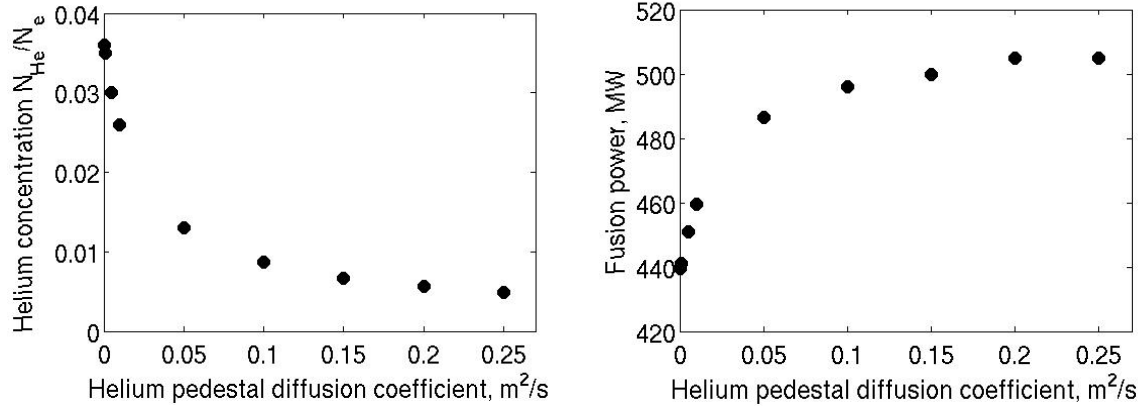


Fig. 8. ILW H-He discharge 101448, impact of central He source on density peaking: electron (black), He (blue) and H (red) densities (top left panel), electron (blue) and ion (red) temperatures (top right panel) and total (black) and neoclassical (magenta) convective velocities (bottom panel) obtained in simulations with the GLF23 model and He NBI fuelling replaced with the He gas puff (dashed curves). The NBI heating remains the same in these simulations. Reference case with 47.6% H and 24.4 % He concentration (Fig. 7) is shown by solid curves for comparison.



*Fig. 9. Simulations of He ash accumulation in the ARC burn phase: He ash concentration  $N_{He}/N_e$  (left panel) and fusion power (right panel) as the functions of the He pedestal diffusion coefficient.  $D_{BgB}/\chi_{e,BgB}(He) = 0.75$  and  $A=0.3$  in these simulations.*